Genetic Algorithm-based Tunings for Baro-fused Inertial Navigation Systems

1st Vinícius M. G. B. Cavalcanti
Diretoria de Ensino, Pesquisa e Extensão
Instituto Federal Fluminense
Itaboraí, RJ, Brazil
vinicius.cavalcanti@gsuite.iff.edu.br

2nd Felipe O. Silva
Department of Automatics
Federal University of Lavras
Lavras, MG, Brazil
felipe.oliveira@ufla.br

3rd Danilo A. de Lima
Department of Automatics
Federal University of Lavras
Lavras, MG, Brazil
danilo.delima@ufla.br

***Abstract*—Information fusion is of paramount importance for sensitive navigation applications. Inertial Navigation Systems (INS) and barometers are two examples of navigation systems/sensors that have complementary error characteristics, and which benefit from such integration. This works revisits two well-established fusion algorithms between the aforementioned systems/sensors, namely, one based on closed-loop mechanizations, and the second based on the Extended Kalman Filter (EKF). Historically, performance of such approaches has shown to be sub-optimal due to the excess of empiricism involved in the associated tuning procedures. In this sense, novel Genetic Algorithm (GA)-based tunings for both approaches are investigated, and results from experimentally conducted tests show their superiority for stabilizing the vertical channel error response of the baro-fused INS. As a requirement for the latter, however, one sees the need for employing raw sensor data sets (in the optimization procedure) that correspond to the dynamics and sensor grade of the application at hand.**

***Index Terms*—Navigation, Inertial, Barometer, Mechanization, Kalman Filter, Information Fusion, Genetic algorithm**

I. Introduction

Navigation is the science that deals with the determination of the attitude, velocity, and position of a moving body, usually a vehicle, w.r.t. a known reference [1], which we refer to as a navigation solution. Generally, one wants to estimate the vehicle's navigation solution accurately, reliably, and at a sufficiently high sampling rate and bandwidth [2]. Such requirements are often achieved using fused (aided, or yet integrated) navigation systems [3], [4], which combine information/data from distinct sources to perform better than the latter would do individually. Usually, the benefits and drawbacks of each information/data source are complementary, thus in a fused navigation system, the advantages of both technologies are combined to improve safety and to provide high-precision and high-accuracy vehicle positioning [5].

There are two main classes of navigation systems [1], [6]: position fixing and dead reckoning. The first class directly determines the instantaneous position of the vehicle from external signals and/or environmental features, e.g. Global Navigation Satellite Systems (GNSS), magnetometers, and barometers; while the second class determines the user position based on the numerical integration of velocity and/or acceleration measurements, e.g. Inertial Navigation Systems (INS) and odometers. The main advantage of an INS lies in its complete independence from external signals. Indeed, the INS solution only depends on three steps [6], [7]: (a) to collect readings from accelerometers and rate gyros that compose its Inertial Measurement Unit (IMU), at a high sampling rate; (b) to numerically integrate those readings; and (c) to add the latter increments to the corresponding navigation solution variables obtained at the preceding time instant. The main INS solution disadvantage, in turn, relates to its inherent error accumulation, which [1]: (a) along the horizontal channel, increases rapidly over time (short-term behavior), but has a medium-to-long term oscillatory nature, which is well characterized by the Schuler frequency; and (b) along the vertical channel, i.e. altitude and vertical velocity, increases unboundedly.

As previously mentioned, fused navigation can be used to limit the increase of INS vertical channel errors. Nowadays, INS/GNSS [8] fusion is widely employed to provide real-time accurate navigation solutions [9]–[12]. Nonetheless, as pointed out in [13], GNSS signals may not be available all the time, or instead, may be corrupted, either accidentally, e.g. due to blockage or multipath propagation, or maliciously, e.g. due to jamming or spoofing. Under those circumstances, and particularly for applications extending over several minutes, a standalone INS vertical solution will certainly violate the applicable accuracy requirements (mainly due to the vertical channel error unstable dynamics) [7], [14]. To circumvent such an issue, INSs have historically been fused with barometers (see e.g. [6], [14]–[21] and references therein), and other external vertical channel reference devices, e.g. [22]–[24].

This work, in particular, deals with the integration of barometer with INS, mainly aiming at investigating the performance of two specific fusion algorithms: (a) one based on control-loops, hereinafter referred to as mechanizations; and (b) the second based on the Extended Kalman Filter (EKF). Both algorithms rely on parameter tuning/optimization, i.e. choosing suitable values for the mechanization gains or the

This study was financed in part by the Research Development Foundation (FUNDEP-MOVER), under grant 27192.02.02/2021.01.00, in part by the Brazilian Agricultural Research Corporation (EMBRAPA), under grant 212-20/2018, in part by the Brazilian National Council for Scientific and Technological Development (CNPq), under grant 312194/2022-6, and in part by the Minas Gerais State Agency for Research and Development (FAPEMIG), under grants APQ-01449-17 and APQ-04659-22.

EKF system noise density and covariance matrices. Generally, manual tuning in an *ad-hoc* basis does not provide optimal outcomes, besides representing a considerable burden to the engineer/designer, and should be preferably avoided.

Decision-making has been moving towards the use of intelligent computational tools [25]. Traditional optimization, e.g. gradient descent, depends upon deterministic iterations and existence of derivatives, which may lead to local optima in nonlinear problems [26]. In contrast, Genetic Algorithms (GA) have been successfully used to find stochastically near optimal solutions (possibly better than local optima) to many engineering problems [27]. Aiming at the latter, Cavalcanti *et al.* [14] recently proposed to solve the baro-INS mechanization problem via GA [27]. Likewise, in this work, we propose a novel GA-based method for the baro-fused INS EKF tuning problem. The very aim of this work, in this sense, is to compare the latter with the GA-tuned baro-INS mechanization of [14] and to evaluate their performances based on statistical measures. As the main contribution of this work, we show that the GA-tuned mechanization performs better than its GA-tuned EKF counterpart, provided that it employs (in the optimization procedure) raw sensor data sets that correspond to the dynamics and sensor grade of the application at hand.

The remainder of this paper is organized as follows: Section II introduces the notation used throughout the paper. In Section III, the problem under investigation is formally stated and the two aforementioned baro-INS fusion methods are recapped. The optimization approaches proposed to tune the latter are presented in Section IV. Some results from experimental tests are discussed in Section V. Finally, Section VI provides concluding remarks.

II. Notation

The following notation is adopted throughout this paper: for a given variable x, $x^n_{eb,U}$ means its Up component, defined for the body frame b w.r.t. the origin of the Earth-Centered-Earth-Fixed (ECEF) frame e and resolved about a local navigation frame n, that could be either North-East-Down (NED) or East-North-Up (ENU). Whenever applicable, subscript i is used to refer to the Earth-Centered Inertial (ECI)-frame. An error in the variable x is denoted by δx, meaning the difference between an estimated $\hat{x}$ or measured $\tilde{x}$ solution, and the ground-truth or reference solution (assumed to be close enough to the real value). For sampled sensor signals, represented by the finite data set $u = \{u_1, \ldots, u_M\}$, $\sigma(u)$ means its standard deviation, while $\sigma_{A,u}$ is the associated Allan standard deviation. The notation $[\mathbf{v}\times]$ represents the skew-symmetric matrix form of vector $\mathbf{v}$. The closed-loop transfer function mapping $\mathbf{w}$ into $\mathbf{z}$ is denoted $\mathbf{T}_{\mathbf{zw}}(s)$. For a given matrix $\mathbf{A}$, $\lambda_i(\mathbf{A})$ denotes its ith eigenvalue.

III. Baro-INS Fusion Algorithms

The purpose of this Section is to briefly introduce the limitations associated with the measurements/estimates of the altitude information via IMUs and barometers. It also conceptualizes the mathematical aspects of two baro-fused INS algorithms that are typically employed to attenuate the vertical channel error growth of a pure INS.

A. Altitude Measurements

Without loss of generality, in a pure INS, the vertical velocity $v^n_{eb,U}$ is computed by integrating the total acceleration of the vehicle in the upward direction $a^n_{eb,U}$, which is obtained by summing the transformed (i.e. upward) specific force acceleration sensed by the strapdown accelerometers $f^n_{ib,U}$ with a suitable gravity model [1]. Altitude h_b, in sequence, is obtained by integrating the vertical velocity. As already pointed out, such INS vertical channel solutions' error growth is unbounded. More precisely, any pre-existing positive altitude error δh_b, which might have been caused, for instance, by an accelerometer error when transforming the specific force into total acceleration, leads to an underestimated local gravity magnitude; thereby, a virtual upward vertical acceleration arises. The latter, when doubly integrated, causes the altitude error to increase even more. By neglecting the cross-coupling between horizontal and vertical channels, the effect of such positive feedback can be approximately modeled as [6], [7], [28]:

$$\frac{h_b(s)}{a^n_{eb,U}(s)} \approx \frac{1}{s^2 - \frac{2g}{r_b}}, \tag{1}$$

where g is the local gravity acceleration magnitude and r_b is the Earth radius at the vehicle location. Note that one of the poles of (1) is $\lambda = \sqrt{2g/r_b}$, which, being positive, corroborate the aforementioned unstable dynamics.

Such an issue is commonly addressed by using an external aiding device that provides an altitude reference to stabilize the INS vertical channel. Here, the reference is provided by barometers, which measure the ambient air pressure p_β to indirectly determine the altitude h_β via, for instance, a standard atmospheric model, such as [29]:

$$h_\beta = \frac{T_{\text{ref}}}{k_T}\left[\left(\frac{p_\beta}{p_{\text{ref}}}\right)^{-\frac{R_{\text{air}}k_T}{g_0}} - 1\right] + h_{\text{ref}}, \tag{2}$$

where p_{ref}, T_{ref}, and h_{ref} are the pressure, temperature, and geodetic altitude at a given reference point, $R_{\text{air}} = 287.05307$ (J/kg K) is the dry air gas constant, $k_T = 6.5\text{E}{-}3$ (K/m) is the atmospheric temperature gradient, and $g_0 = 9.80665$ (m/s^2) is the standard acceleration due to gravity. Although barometers provide bounded solutions for vehicle altitude estimation, their measurements suffer from lags during sharp climbs and dives, as well as significant noise, low resolution, and errors arising from differences between the true and modeled atmosphere [1], [28], [29].

Given the complementary nature of their errors, INS and barometers are good candidates for the sensory fusion algorithms discussed hereinafter.

B. Baro-fused INS via Mechanization

In this method, the altitude solution h_b (provided by the INS) is compared with a reference altitude h_β (provided by the barometer), and then fed back via suitable gains, in a

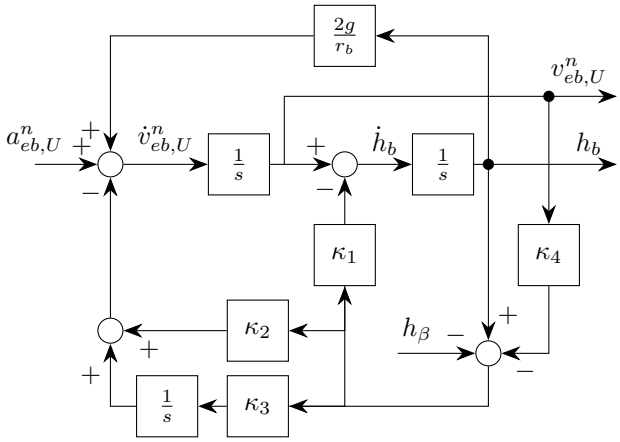

Fig. 1. Third-order vertical channel mechanization with four gains.

servomechanism fashion, to stabilize the vertical channel, as depicted in Fig. 1. More precisely, Fig. 1 depicts a 3rd-order Two-Input Two-Output (TITO) mechanization with four gains, which can be considered the most generic and flexible interconnection for vertical channel damping [6]. Following [7], [14], the mechanization problem can be stated as follows:

Problem 1. Find a suitable set of gains $\boldsymbol{\kappa} \in \mathbb{R}^4$ for the interconnection depicted in Fig. 1, such that the TITO system is stable and the magnitudes of the gains are: (a) large enough to suitably bound low-frequency signals due to accelerometer errors; and (b) small enough to dampen high-frequency signals due to barometer errors.

In this sense, the mechanization gain selection is a trade-off between objectives (a) and (b) on Problem 1, aiming to bound INS vertical channel errors and achieve satisfactory response even in the presence of barometer disturbances. This task relies on the designer's skill and experience, hence heuristics, i.e. trial-and-error or rule of thumb, is frequently adopted. Most of the literature on the subject, in turn, proposes a combination of heuristics and classic control theory for tuning purposes, e.g. as in [7], [24], [28], [30]–[33]. More recently, other approaches were also investigated: (a) methods based on optimal control theory, with the Linear Quadratic Regulator (LQR) approach standing out [6]; and (b) a method based on evolutionary multi-objective optimization [14].

C. Baro-fused INS via EKF

As an alternative approach to the baro-fused INS mechanization of Section III-B, barometric and IMU measurements can also be integrated, aiming at the attenuation of the vertical channel error growth, via a closed-loop error-state Tightly-Coupled (TC) EKF using NED navigation equations[1] [1]. Consider that the latter is described by the following dynamic model:

$$\begin{aligned}\dot{\mathbf{x}}(t) &= \mathbf{F}(t)\mathbf{x}(t) + \mathbf{G}(t)\mathbf{w}_x(t),\\ \mathbf{y}(t) &= \mathbf{H}(t)\mathbf{x}(t) + \mathbf{w}_y(t).\end{aligned} \tag{3}$$

[1]Despite adopting NED frame in the EKF, what we are interested in is the vertical channel solution in the Up direction, that is straightforward to assess as (a) the altitude $\hat{h}_b$ is already defined pointing Up; and (b) the downward velocity is simply the opposite of the upward velocity, i.e. $\hat{v}^n_{eb,U} = -\hat{v}^n_{eb,D}$.

Let the state vector be defined by the errors in the INS-computed attitude $\delta\boldsymbol{\Psi}^n_{nb}$, velocity $\delta\mathbf{v}^n_{eb}$, and curvilinear position $\delta\mathbf{p}_b$ solution, in addition to the accelerometer bias $\mathbf{b}_a$, rate gyro bias $\mathbf{b}_g$, barometer bias b_β and barometer scale factor error s_β:

$$\mathbf{x} \triangleq \begin{bmatrix}(\delta\boldsymbol{\Psi}^n_{nb})^T & (\delta\mathbf{v}^n_{eb})^T & \delta\mathbf{p}_b^T & \mathbf{b}_a^T & \mathbf{b}_g^T & b_\beta & s_\beta\end{bmatrix}^T, \tag{4}$$

with

$$\delta\mathbf{p}_b^T \triangleq \begin{bmatrix}\delta L_b & \delta\lambda_b & \delta h_b\end{bmatrix}, \tag{5}$$

where δL_b and $\delta\lambda_b$ are the INS latitude and longitude errors, respectively.

The EKF system matrix can be modeled as [1]

$$\mathbf{F} = \begin{bmatrix} -[\hat{\boldsymbol{\omega}}^n_{in}\times] & \mathbf{F}_{12} & \mathbf{F}_{13} & \mathbf{0}_3 & \hat{\mathbf{C}}^n_b & 0 & 0\\ -[\hat{\mathbf{C}}^n_b\mathbf{f}^b_{ib}\times] & \mathbf{F}_{22} & \mathbf{F}_{23} & \hat{\mathbf{C}}^n_b & \mathbf{0}_3 & 0 & 0\\ \mathbf{0}_3 & \mathbf{F}_{32} & \mathbf{F}_{33} & \mathbf{0}_3 & \mathbf{0}_3 & 0 & 0\\ \mathbf{0}_3 & \mathbf{0}_3 & \mathbf{0}_3 & \mathbf{F}_{44} & \mathbf{0}_3 & 0 & 0\\ \mathbf{0}_3 & \mathbf{0}_3 & \mathbf{0}_3 & \mathbf{0}_3 & \mathbf{F}_{55} & 0 & 0\\ \mathbf{0}_3 & \mathbf{0}_3 & \mathbf{0}_3 & \mathbf{0}_3 & \mathbf{0}_3 & F_{66} & 0\\ \mathbf{0}_3 & \mathbf{0}_3 & \mathbf{0}_3 & \mathbf{0}_3 & \mathbf{0}_3 & 0 & 0\end{bmatrix}, \tag{6}$$

with[2]

$$\mathbf{F}_{12,3} = \begin{bmatrix}0 & \frac{\tan(\hat{L}_b)}{R_E(\hat{L}_b)+\hat{h}_b} & 0\end{bmatrix}, \tag{7}$$

$$\mathbf{F}_{13,3} = \begin{bmatrix}\omega_{ie}\cos\left(\hat{L}_b\right) + \frac{\hat{v}^n_{eb,E}}{\left(R_E(\hat{L}_b)+\hat{h}_b\right)\cos^2(\hat{L}_b)}\\ 0\\ -\frac{\hat{v}^n_{eb,E}\tan(\hat{L}_b)}{\left(R_E(\hat{L}_b)+\hat{h}_b\right)^2}\end{bmatrix}^T, \tag{8}$$

$$\mathbf{F}_{22,3} = \begin{bmatrix}-\frac{2\hat{v}^n_{eb,N}}{\left(R_N(\hat{L}_b)+\hat{h}_b\right)^2}\\ -\frac{2\hat{v}^n_{eb,E}}{\left(R_E(\hat{L}_b)+\hat{h}_b\right)^2} - 2\omega_{ie}\cos\left(\hat{L}_b\right)\\ 0\end{bmatrix}^T, \tag{9}$$

$$\mathbf{F}_{32,3} = \begin{bmatrix}0 & 0 & -1\end{bmatrix}, \tag{10}$$

$$\mathbf{F}_{33,3} = \begin{bmatrix}0 & 0 & 0\end{bmatrix}, \tag{11}$$

$$\mathbf{F}_{44,3} = \begin{bmatrix}0 & 0 & -\frac{1}{\hat{T}_{B,a}}\end{bmatrix}, \tag{12}$$

$$\mathbf{F}_{55,3} = \begin{bmatrix}0 & 0 & -\frac{1}{\hat{T}_{B,g}}\end{bmatrix}, \tag{13}$$

$$F_{66} = -\frac{1}{\hat{T}_{B,\beta}}, \tag{14}$$

where $\boldsymbol{\omega}^n_{in}$ is the angular rate vector of NED frame w.r.t. the inertial frame, resolved on NED frame axes; $\mathbf{C}^n_b$ is the direction cosine matrix between body and NED frames; R_N and R_E are the meridian and transverse radii of curvature of Earth, respectively; ω_{ie} is the Earth's angular rate magnitude; and $T_{B,a}$, $T_{B,g}$, and $T_{B,\beta}$ are the correlation times of the accelerometer, rate gyro, and barometer instability biases, respectively, modeled here as 1st-order Gauss-Markov processes [2].

[2]For the sake of simplicity, only the EKF system matrix rows associated with the vertical channel dynamics have been depicted in this paper, i.e. (7) to (14) only depict the third row of their corresponding sub-matrices.

The system noise distribution matrix is modeled as

$$\mathbf{G} = \begin{bmatrix} \mathbf{G}' \\ \mathbf{0}_{1\times 16} \end{bmatrix}, \tag{15}$$

with

$$\mathbf{G}' = \text{diag}\left\{ \hat{\mathbf{C}}_b^n,\, \hat{\mathbf{C}}_b^n,\, \mathbf{0}_3,\, \mathbf{I}_3,\, \mathbf{I}_3,\, 1 \right\}. \tag{16}$$

Next, and particularly for the TC EKF approach, the measurement is a scalar, which is defined as the difference between the barometric pressure $\tilde{p}_\beta$ and its estimate from the INS solution:

$$y(t) \triangleq \tilde{p}_\beta - \hat{p}_\beta\left(\hat{h}_b\right), \tag{17}$$

where $\hat{p}_\beta\left(\hat{h}_b\right)$ is estimated from the inverse function of (2), based on the INS-computed altitude $\hat{h}_b$.

The measurement matrix is modeled as

$$\mathbf{H} = \begin{bmatrix} \mathbf{0}_{1\times 8} & H' & \mathbf{0}_{1\times 6} & 1 & \hat{p}_\beta\left(\hat{h}_b\right) \end{bmatrix}, \tag{18}$$

with

$$H' = \frac{g_0 p_{\text{ref}}}{R_{\text{air}} T_{\text{ref}} \left(\frac{k_T\left(\hat{h}_b - h_{\text{ref}}\right)}{T_{\text{ref}}} + 1 \right)^{\frac{g_0}{k_T}+1}}. \tag{19}$$

Once estimated, the INS error states are fed back into the INS solution, and used to correct the latter (closed-loop error-state implementation), while the IMU and aiding sensor error states (biases and scale factor error) are used to calibrate the sensor outputs in subsequent epochs.

In general, the design parameters of such an EKF are the correlation times in (12) to (14), the system noise density matrix

$$\mathbf{S} = \text{diag}\left\{ \mathbf{I}_3\hat{S}_{N,g},\, \mathbf{I}_3\hat{S}_{N,a},\, \mathbf{0}_3,\, \mathbf{I}_3\hat{S}_{B,g},\, \mathbf{I}_3\hat{S}_{B,a},\, \hat{S}_{B,\beta} \right\}, \tag{20}$$

and the measurement noise covariance matrix (a scalar, in this particular case)

$$R = \frac{\hat{S}_{N,\beta}}{\tau}, \tag{21}$$

with $\hat{S}_{N,g}$, $\hat{S}_{N,a}$, and $\hat{S}_{N,\beta}$, being, respectively, the estimates of the Power Spectral Densities (PSD) of the rate gyro, accelerometer, and barometer random noises; and $\hat{S}_{B,g}$, $\hat{S}_{B,a}$, and $S_{B,\beta}$, the PSDs of the rate gyro, accelerometer, and barometer instability bias driven noises, also respectively.

As in the baro-fused INS mechanization of Section III-B, proper tuning of (20) and (21) requires skill and experience from the designer, and/or suitable previous error characterization from the sensor manufacturers, which is not always at hand. The next Section discusses a stochastic noise characterization technique that is useful to tackle such a situation.

D. ASD Plot-based EKF Tuning

In compliance with standards [34], IMU manufacturers are expected to supply sufficiently informative data sheets that characterize their sensors w.r.t. their stochastic performance, and this is typically stated in terms of the Allan Variance (AV) plot [35], Allan Standard Deviation (ASD) plot, or parameters extracted from them. When the manufacturer does not provide an ASD plot (or provides information that the designer considers insufficient), the designer then shall acquire his/her own data set to construct the ASD plots, as done in [36].

Let $\tilde{u} = \{\tilde{u}_1, \ldots, \tilde{u}_M\}$ be a given data set measured at a constant sampling interval T for a stationary IMU (or barometer). For each $k = [1,\, M/2]$, the AV is computed for values of cluster time $\tau_c = kT$ ranging from T to $MT/2$. Given k, at each time instant $t_i \in [T,\, 2T,\, \ldots,\, (M-k)T]$, a set $\tilde{u}_j = \{\tilde{u}_i,\, \ldots,\, \tilde{u}_{i+k-1}\}$ forms a cluster. For each cluster, an average value is computed as

$$\overline{u}_i(\tau_c) = \frac{1}{k}\sum_{j=0}^{k-1} \tilde{u}_{i+j}. \tag{22}$$

Finally, the AV for each τ_c is then computed as

$$\sigma^2_{A,u}(\tau_c) = \frac{1}{2(M-2k)} \sum_{i=1}^{M-2k} \left(\overline{u}_{i+k}(\tau_c) - \overline{u}_i(\tau_c)\right)^2, \tag{23}$$

from which the corresponding ASD can be extracted from the direct application of the square root.

It is not immediately clear though, how to translate the AV (or ASD) plot into suitable information to characterize the IMU (or barometer) stochastic errors. Next, and aiming at the latter, one recaps the overall sensor (either IMU or barometer) model recently proposed by Farrell *et al.* [2], namely:

$$\tilde{u}(t) = u(t) + d(u(t)) + z(t), \tag{24}$$

with

$$z(t) \triangleq z_N(t) + z_B(t) + z_K(t), \tag{25}$$

where $\tilde{u}(t)$ is a measurement of the desired signal $u(t)$, which is corrupted both by deterministic errors $d(u(t))$ and by cumulative stochastic errors $z(t)$.

The first term in (25) is a white Gaussian random noise affecting the sensor, i.e.

$$z_N(t) \triangleq w_N(t), \tag{26}$$

with PSD S_N, which yields [34]

$$\sigma^2_{A,N}(\tau_c) = \frac{S_N}{\tau_c}. \tag{27}$$

The second term in (25) relates to a bias instability affecting the sensor. Even though there is no finite-order linear state-space model for the latter [2], it may be approximated by a first-order Gauss-Markov process [37], [38], i.e.

$$\dot{z}_B(t) \approx -\frac{1}{T_B} z_B(t) + w_B(t), \tag{28}$$

where T_B is the process correlation time, and $\omega_B(t)$ is the process driving white noise with PSD S_B, which yields [34]

$$\sigma^2_{A,B}(\tau_c) = \frac{S_B T_B^2}{\tau_c}\left[1 - \frac{T_B}{2\tau_c}\left(3 - 4e^{-\frac{\tau_c}{T_B}} + e^{-\frac{2\tau_c}{T_B}}\right)\right]. \tag{29}$$

The third term in (25), lastly, represents a random walk affecting the sensor, i.e.

$$\dot{z}_K(t) \triangleq w_K(t), \tag{30}$$

where $\omega_K(t)$ is a white Gaussian random noise with PSD S_K, which yields [34]

$$\sigma^2_{A,K}(\tau_c) = \frac{S_K \tau_c}{3}. \tag{31}$$

Accordingly, from (25), (26), (28) and (30), the cumulative error model of terms N, B, and K in state-space form is given by

$$\begin{array}{rcl} \begin{bmatrix} \dot{z}_B(t) \\ \dot{z}_K(t) \end{bmatrix} & = & \begin{bmatrix} -\frac{1}{T_B} & 0 \\ 0 & 0 \end{bmatrix} \begin{bmatrix} z_B(t) \\ z_K(t) \end{bmatrix} + \begin{bmatrix} w_B(t) \\ w_K(t) \end{bmatrix}, \\ z(t) & = & \begin{bmatrix} 1 & 0 \\ 0 & 1 \end{bmatrix} \begin{bmatrix} z_B(t) \\ z_K(t) \end{bmatrix} + w_N(t). \end{array} \tag{32}$$

Also, and considering that the AV for each type of noise is additive, one has that

$$\sigma^2_{A,z}(\tau_c) = \sigma^2_{A,N}(\tau_c) + \sigma^2_{A,B}(\tau_c) + \sigma^2_{A,K}(\tau_c), \tag{33}$$

where the right-side terms are defined in (27), (29) and (31) respectively. The problem of selecting the sensor stochastic error parameters from the AV (or ASD) plot can be stated as follows:

Problem 2. Find suitable parameters S_N, S_B, S_K, and T_B such that the model (33) fits the AV (or ASD) plot for a measured sensor data set $\tilde{u}$.

Once selected (for both the IMU and barometer), S_N, S_B, S_K, and T_B can be used to tune the baro-fused INS EKF. In general, such parameters are chosen visually from the AV (or ASD) plot and independently, i.e. neglecting (33). As an alternative, Farrell *et al.* [2] recently proposed to adjust the latter jointly, via a Weighted Least Squares (WLS) approach. In this paper, we propose a GA-based optimization approach, which is described in the next Section.

IV. Genetic Algorithm-based Tunings

In this Section we propose optimization tools to solve Problem 1 (Section III-B) and Problem 2 (Section III-D). Due to space limitations, the reader is invited to refer to [27], [39] and their references for details on GA-based optimization.

A. Mechanization Tuning

In this Section, we briefly summarize the GA-based solution for the baro-fused INS mechanization, as recently proposed in [14]. Consider that the mapping from $\mathbf{w}_v \triangleq [a^n_{eb,U}\; h_\beta]^T$ to $\mathbf{z}_v \triangleq [v^n_{eb,U}\; h_b]^T$ for the close-loop TITO system depicted in Fig. 1 admits a state-space realization of the form:

$$\mathbf{T}_{\mathbf{z}_v \mathbf{w}_v}(s;\kappa) = \left[\begin{array}{c|c} \mathbf{A}(\boldsymbol{\kappa}) & \mathbf{B}(\boldsymbol{\kappa}) \\ \hline \mathbf{C}(\boldsymbol{\kappa}) & \mathbf{D}(\boldsymbol{\kappa}) \end{array}\right], \tag{34}$$

where $\boldsymbol{\kappa} \in \mathbb{R}^4$ represents a vector of tunable gains. Also, assume that the designer has experimental data sets, which can represent the final application well enough.

Problem 1 can be solved by minimizing a vector cost-function whose components are the standard deviations (SD) of the altitude and the vertical velocity error responses over time. Thus, Problem 1 can be translated into the following multi-objective constrained program:

$$\begin{array}{ll} \underset{\boldsymbol{\kappa}}{\text{minimize}} & \left[\sigma(\delta h_b(\boldsymbol{\kappa})) \quad \sigma(\delta v^n_{eb,U}(\boldsymbol{\kappa}))\right], \\ \text{subject to} & \max_i \operatorname{Re}\{\lambda_i(\mathbf{A}(\boldsymbol{\kappa}))\} < 0, \\ & |\kappa_j| \le c, \quad c > 0, \quad \forall j \in \{1,2,3,4\}. \end{array} \tag{35}$$

A variant of the NSGA-II [40] can be used to search Pareto-optimal solutions for (35). Afterward, the objectives are normalized in the range $[0,\, 1]$. Then, the solution with the minimum L_2-norm is selected, as suggested in [41]. Note that this work is not intended to provide a sensitivity analysis of the solutions over the Pareto front. The discussion, instead, is restricted to performance comparisons (see Section V).

B. EKF Tuning

Considering the state-space model (32), a possible parameterization for the estimated AV model (33) is given by

$$\hat{\sigma}^2_{A,z}(\tau_c, \boldsymbol{\theta}) = \frac{\theta_1}{\tau_c} + \frac{\theta_2 \theta_4^2}{\tau_c}\left[1 - \frac{\theta_4}{2\tau_c}\left(3 - 4e^{-\frac{\tau_c}{\theta_4}} + e^{-\frac{2\tau_c}{\theta_4}}\right)\right] + \frac{\theta_3 \tau_c}{3}, \tag{36}$$

where $\boldsymbol{\theta} \triangleq [S_N\, S_B\, S_K\, T_B]$.

The cost-function proposed by Farrell *et al.* [2] to Problem 2 was defined as a cluster-time-weighted function of the squared difference between the experimentally measured AV and the parameterized AV of eq. (36), i.e.

$$f(\boldsymbol{\theta}) \triangleq \sum_{i=1}^{M} W_i \left[\tilde{\sigma}^2_{A,z}(\tau_{c,i}) - \hat{\sigma}^2_{A,z}(\tau_{c,i};\boldsymbol{\theta})\right]^2, \tag{37}$$

where

$$W_i = \frac{1}{\left(2\sqrt{\frac{k}{2M}}\tilde{\sigma}_{A,z}(\tau_{c,i})\right)^2}. \tag{38}$$

Problem 2 could be translated into the following single-objective constrained program:

$$\begin{array}{ll} \underset{\boldsymbol{\theta}}{\text{minimize}} & f(\boldsymbol{\theta}), \\ \text{subject to} & \theta_j \ge 0, \quad \forall j \in \{1,2,3,4\}. \end{array} \tag{39}$$

Note that (36) is nonlinear w.r.t. θ_4, therefore Farrell *et al.* [2] suggested to solve (39) by a golden-section search over θ_4 and then solving the remaining parameters via WLS. Alternatively, we propose to solve (39) directly employing GA [27]. It is noteworthy that such framework enables the designer to use previously known good solutions in the initial population to search for better solutions to the problem, and to prevent non-convergence; thus, solutions from the method proposed in [2] and manual tunings were employed in our GA approach.

V. Results

To validate the GA-based tuning methods proposed in Section IV, as well as to compare its performance with state-of-the-art tunings found in the literature, we conducted experimental tests with real data sets. These were collected

using an Xsens MTi-680G module attached to a car at Lavras-MG, Brazil, on July 21, 2023, which executed a wide range of dynamics that are typical for urban scenarios, such as curves, accelerations, decelerations, climbs, descents, stops, and so forth. To evaluate the solutions obtained from each fusion algorithm alongside the corresponding tunings, a double-frequency RTK-enabled Differential GNSS-fused INS via TC EKF was used as the ground-truth (GT).

The optimization procedure described in Section IV-A was performed with the dynamic MTi-680G raw data sets to generate a mechanization estimation of the vertical channel, being, in sequence, compared with the GT solution to compute the optimization objectives. The hyperparameters required to solve (35) using multi-objective GA were set as follows: (a) maximum value $c = 5$ for each of the parameters in the decision vector $\boldsymbol{\kappa}$; (b) population size $n_{\text{pop}} = 50$; and (c) maximum number of generations $n_{\text{gen}} = 200$.

Table I summarizes the final tuning of the investigated baro-fused INS mechanizations, namely: (a) GA_{680} denotes the GA-based tuning, which employed the same raw data collected in the proposed experimental test; (b) GA_{7} denotes the GA-based tuning proposed in [14], which used, during the optimization procedure, a different data set (corresponding to distinct vehicle dynamics) collected with an Xsens MTi-7 module (slightly inferior, in terms of performance, to the MTi-680G); (c) the empirical tuning suggested by Savage [7]; and (d) the optimal LQR tuning proposed in [6].

The optimization procedure described in Section IV-B, in turn, was performed based on stationary MTi-680G raw data sets. The hyperparameters required to solve (39) utilizing GA were set as follows: (a) population size $n_{\text{pop}} = 100$; and (b) maximum number of generations $n_{\text{gen}} = 50$.

Table II summarizes the final costs associated to the sensor stochastic error model tunings, for the EKF-based baro-fused INS approach, namely: (a) manual tuning, which was based on the visual selection of the stochastic error parameters from the experimentally measured AV (or ASD) plots; (b) the WLS approach described in [2]; and (c) the GA-based approach proposed in Section IV-B (best results are highlighted in green color, and worst, in red). For each sensor and tuning method, the cost is associated with a set of parameters S_N, S_B, S_K, and T_B, which are reported in Table III (all PSD values are in the International System of Units (SI)). The experimentally measured ASD plots (for each sensor), as well as the parameterized ones (by each tuning approach), are presented in Figs. 2 to 4. As can be readily verified (and as expected), the proposed GA-based tuning estimated better the ASD parameters for all analyzed sensors.

In sequence, the sensor stochastic error parameters in

TABLE I
FINAL TUNING OF THE BARO-FUSED INS MECHANIZATION GAINS.

Tuning	κ_1 (s^{-1})	κ_2 (s^{-2})	κ_3 (s^{-3})	κ_4 (s)
Savage [7]	0.30	0.03	1.00E–3	0.00
LQR [6]	2.41	2.41	1.00	0.00
GA_{7} [14]	4.72	0.58	6.16E–3	–1.08
GA_{680}	4.30	4.31	1.45E–2	–4.85

TABLE II
COST FOR THE AV PLOT OPTIMIZATION PROBLEM.

Tuning	$f(\boldsymbol{\theta})_{\text{accl}}$	$f(\boldsymbol{\theta})_{\text{gyro}}$	$f(\boldsymbol{\theta})_{\text{baro}}$
Manual	5.66E+11	1.38E+12	3.78E+12
WLS [2]	1.31E+11	9.75E+10	5.08E+14
GA	1.07E+11	9.18E+10	1.06E+12

TABLE III
SELECTED ASD PARAMETERS.

	Tuning	S_N	S_B	S_K	T_B (s)
Accl.	Manual	5.63E–7	4.26E–10	6.40E–11	176.00
	WLS [2]	6.61E–7	5.55E–10	8.21E–11	47.74
	GA	6.31E–7	5.55R–10	6.40E–11	48.14
Gyro.	Manual	3.24E–8	1.25E–11	4.90E–13	519.00
	WLS [2]	3.74E–8	3.03E–11	6.84E–13	558.83
	GA	3.71E–8	2.92E–11	6.73E–13	556.40
Baro.	Manual	1.48E–1	7.05E–2	0.00	3.34
	WLS [2]	1.54E–1	0.00	1.53E–1	44.62
	GA	1.37E–1	1.37E–2	1.80E–2	1.00

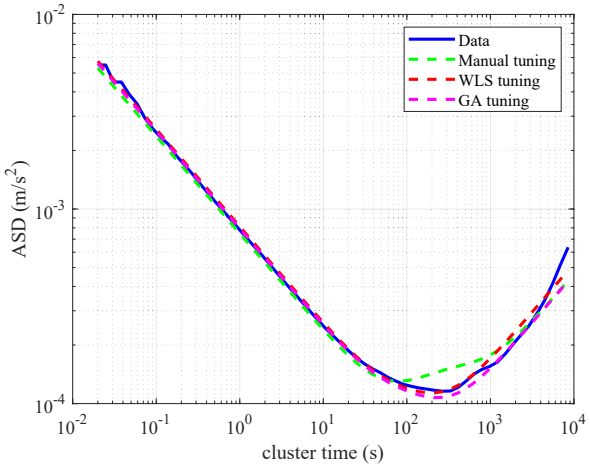

Fig. 2. ASD plots for the MTI-680G accelerometer data.

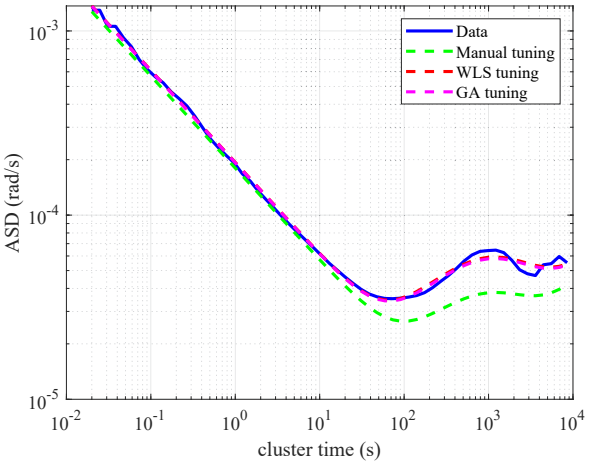

Fig. 3. ASD plots for the MTI-680G rate gyro data.

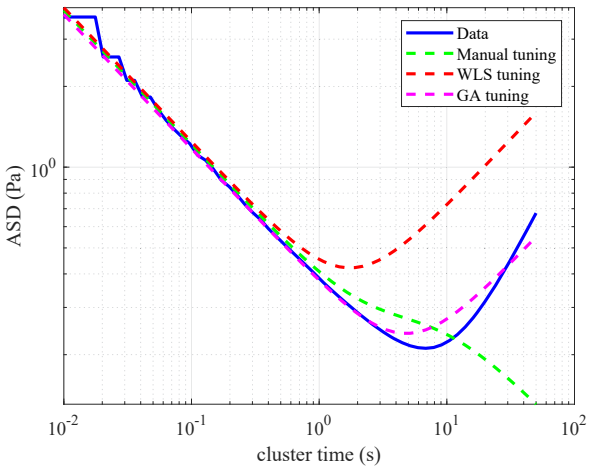

Fig. 4. ASD plots for the MTI-680G barometer data.

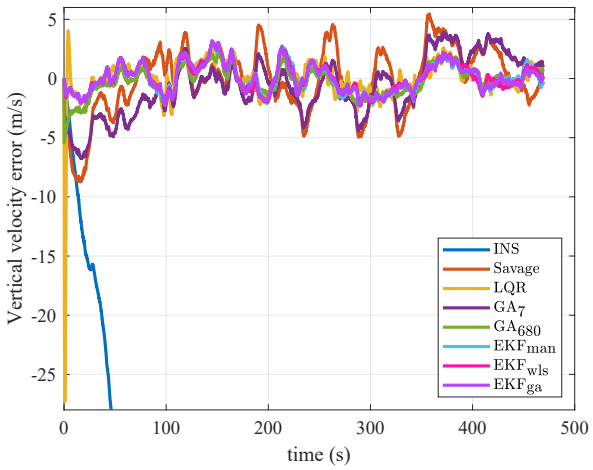

Fig. 6. Vertical velocity error response.

Table III were used to provide different tunings for the baro-fused INS via EKF. Figure 5 depicts the altitude error profiles for each of the investigated fusion algorithms (both mechanization- and EKF-based). It additionally depicts the pure barometer output error. Figure 6, in turn, depicts the vertical velocity errors, for the same algorithms and the pure INS output solution. Table IV provides a collection of performance metrics, which were computed from the signals shown in Figs. 5 and 6. Each metric was considered as an objective to be optimized. As done in Section IV-A and suggested in [41], we also normalized each metric in the range $[0, 1]$ and then computed the L_2-norm of the resulting decision vector, to validate each algorithm/tuning.

As can be seen, the GA-based tunings were the ones that provided the best results in terms of the L_2-norm of the vertical channel errors, both for the mechanization- and EKF-based baro-INS integrations. Worthy of note is the fact that the GA-tuned mechanization proved to perform even better than its GA-tuned EKF counterpart. Such outcome, however, changed dramatically (specifically w.r.t. the vertical velocity error) when the GA-based mechanization employed (for the optimization procedure) raw data that did not correspond to the current vehicle dynamics (see metrics from GA_7). Also interesting is the fact the WLS-tuned EKF solution performed worse than its manual tuning counterpart, which might be related to the bad barometer stochastic error model identification provided by the former (see Fig. 4, for details). Savage-tuned mechanization lastly, was the approach that performed worst, providing an altitude solution that was inferior even to the pure barometric output.

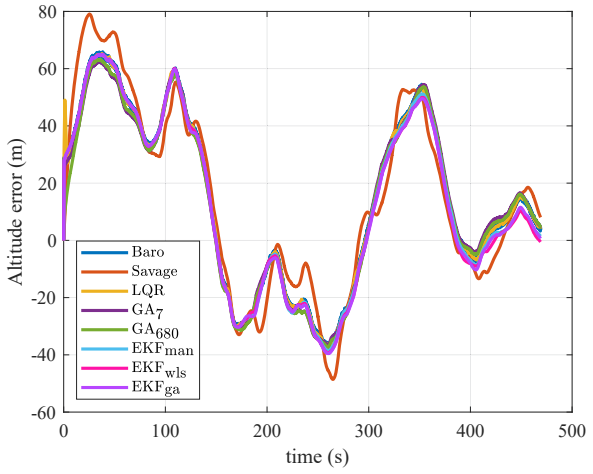

Fig. 5. Altitude error response.

VI. Conclusion

This study reviewed the problem of baro-fused INS algorithms via mechanization and EKF using different tuning methods. As verified in the experimental results, GA-based tunings proved to be effective in improving the vertical channel error response of the latter fusion algorithms, provided that the raw sensor data used in the optimization procedure correspond to the dynamics (for the mechanization tuning) and sensor grade (for both mechanization and EKF tuning) of the application at hand. As suggestions for future works, one has the evaluation/solution of: (a) both mechanization- and EKF-based INS/baro/GNSS fusion algorithms, in the advent of GNSS outages; (b) Problem 1 in terms of variance minimization; and (c) Problem 2 based on other optimization tools.

References

[1] P. D. Groves, *Principles of GNSS, Inertial, and Multisensor Integrated Navigation Systems*, 2nd ed. Artech House Publishers, 2013.

[2] J. A. Farrell, F. O. Silva, F. Rahman, and J. Wendel, "Inertial measurement unit error modeling tutorial: Inertial navigation system state estimation with real-time sensor calibration," *IEEE Contr. Syst. Mag.*, vol. 42, no. 6, pp. 40–66, 2022.

[3] D. Engelsman and I. Klein, "Information-aided inertial navigation: A review," *IEEE T. Instrum. Meas.*, vol. 72, pp. 1–18, 2023.

[4] J. A. Farrell, *Aided Navigation: GPS with High Rate Sensors*. McGraw-Hill, Inc., 2008.

[5] Y. He, J. Li, and J. Liu, "Research on GNSS INS & GNSS/INS integrated navigation method for autonomous vehicles: A survey," *IEEE Access*, vol. 11, pp. 79 033–79 055, 2023.

TABLE IV
VERTICAL CHANNEL ERROR METRICS FOR THE DYNAMIC VEHICLE EXPERIMENT

Metric		Tuning							
		Baro/INS	Savage	LQR	GA_7	GA_{680}	EKF_{man}	EKF_{wls}	EKF_{ga}
Altitude (m)]	Root Mean Square	33.69	36.03	33.73	32.98	32.89	33.50	33.36	33.39
	Peak	65.91	79.05	65.32	62.46	63.23	65.00	65.04	64.96
	Mean	14.60	15.18	14.60	14.05	13.43	13.56	13.02	13.03
	Average Absolute	28.28	29.27	28.32	28.07	27.88	28.00	27.87	27.98
	Standard Deviation	30.36	32.67	30.40	29.84	30.03	30.63	30.72	30.75
	Mean Absolute Deviation	26.76	27.92	26.81	26.11	26.16	27.25	27.37	27.31
Vert. vel. (m/s)	Root Mean Square	163.72	2.78	1.86	2.53	1.24	1.18	1.20	1.18
	Peak	258.74	8.74	27.32	6.76	5.45	2.99	3.18	3.18
	Mean	−142.26	−1.78E–1	1.08E–3	−6.24E-1	−2.50E–1	2.11E-2	4.07E–2	2.54E–2
	Average Absolute	142.26	2.16	1.09	2.05	9.84E–1	1.00	1.01	1.00
	Standard Deviation	81.04	2.78	1.86	2.45	1.21	1.18	1.20	1.18
	Mean Absolute Deviation	72.16	2.16	1.09	2.01	9.69E–1	1.00	1.02	1.00
L_2-norm		N/A	3.18	1.52	2.05	4.64E–1	7.80–1	7.97E–1	7.74–1

[6] L. A. Vieira and F. O. Silva, "Vertical channel stabilization of barometer-aided inertial navigation systems by optimal control," *Asian J. Control*, vol. 25, no. 5, pp. 3395–3411, 2023.

[7] P. G. Savage, *Strapdown Analytics*, 1st ed. Strapdown Associates, 2000.

[8] J. A. Farrell and J. Wendel, "GNSS/INS integration," in *Springer Handbook of Global Navigation Satellite Systems*, P. J. Teunissen and O. Montenbruck, Eds. Springer, Cham, 2017, pp. 811–840.

[9] A. da Silva and J. da Cruz, "Fuzzy adaptive extended Kalman filter for UAV INS/GPS data fusion," *J Braz. Soc. Mech. Sci. Eng.*, vol. 38, p. 1671–1688, 2016.

[10] E. L. V. Hinüber, C. Reimer, T. Schneider, and M. Stock, "INS/GNSS integration for aerobatic flight applications and aircraft motion surveying," *Sensors*, vol. 17, no. 5, 2017.

[11] T.-S. Lou, N.-H. Chen, Z.-W. Chen, and X.-L. Wang, "Robust partially strong tracking extended consider Kalman filtering for INS/GNSS integrated navigation," *IEEE Access*, vol. 7, pp. 151 230–151 238, 2019.

[12] C. Hajiyev, U. Hacizade, and D. Cilden-Guler, "Integration of barometric and gps altimeters via adaptive data fusion algorithm," *International Journal of Adaptive Control and Signal Processing*, vol. 35, no. 1, pp. 2–14, 2021.

[13] E. Gallo and A. Barrientos, "Reduction of GNSS-denied inertial navigation errors for fixed wing autonomous unmanned air vehicles," *Aerosp. Sci. Technol.*, vol. 120, p. 107237, 2022.

[14] V. M. G. B. Cavalcanti, F. O. Silva, Á. H. A. Maia, D. A. de Lima, A. C. Leite, and J. A. Farrell, "Evolutionary optimization for tuning barometer-aided inertial navigation system vertical channel mechanization," in *SBAI 2023*, 2023, pp. 1–8.

[15] A. M. Sabatini and V. Genovese, "A sensor fusion method for tracking vertical velocity and height based on inertial and barometric altimeter measurements," *Sensors*, vol. 14, no. 8, pp. 13 324–13 347, 2014.

[16] Y. Son and S. Oh, "A barometer-IMU fusion method for vertical velocity and height estimation," in *2015 IEEE SENSORS*, 2015, pp. 1–4.

[17] S. Wei, G. Dan, and H. Chen, "Altitude data fusion utilising differential measurement and complementary filter," *IET Science, Measurement & Technology*, vol. 10, no. 8, pp. 874–879, 2016.

[18] A. M. Contreras and C. Hajiyev, "Integration of baro-inertial-GPS altimeter via complementary Kalman filter," in *Advances in Sustainable Aviation*, T. H. Karakoç, C. O. Colpan, and Y. Şöhret, Eds. Springer, Cham, 2018, pp. 251–267.

[19] L. A. Vieira, F. O. Silva, R. P. Menezes Filho, and L. P. S. Paiva, "Performance indices-based tuning for barometer-aided inertial navigation systems," in *Latin American Robotics Symp.* IEEE, 2020, pp. 1–6.

[20] F. O. Silva and L. A. Vieira, "Optimizing the gains of baro-inertial vertical channel mechanizations," in *Proc. 31st Int. Symp. Industrial Electronics*. IEEE, 2022, pp. 582–588.

[21] X. Zhao, Y. Meng, F. Qi, L. Wang, and X. Zhu, "A vertical channel-enhanced fusion method based on RINS and barometric altimeter for UAVs in GNSS denial environments," *IEEE T. Instrum. Meas.*, vol. 72, pp. 1–12, 2023.

[22] C. Hajiyev, "Fault tolerant integrated radar/inertial altimeter based on nonlinear robust adaptive Kalman filter," *Aerosp. Sci. Technol.*, vol. 17, no. 1, pp. 40–49, 2012.

[23] L. Zhang, Z. Zhai, L. He, P. Wen, and W. Niu, "Infrared-inertial navigation for commercial aircraft precision landing in low visibility and GPS-denied environments," *Sensors*, vol. 19, no. 2, 2019.

[24] Y. Ben, W. Cui, and Q. Li, "A new gains-selection method of depth gauge aided vertical channel for underwater vehicles," *Measurement*, vol. 214, p. 112761, 2023.

[25] W. Pedrycz, N. Ichalkaranje, G. Phillips-Wren, and L. C. Jain, "Introduction to computational intelligence for decision making," in *Intelligent Decision Making: An AI-Based Approach*, G. Phillips-Wren, N. Ichalkaranje, and L. C. Jain, Eds. Springer, Berlin, Heidelberg, 2008, pp. 79–96.

[26] D. E. Goldberg, *Genetic Algorithms in Search, Optimization, and Machine Learning*, 1st ed. Addison-Wesley Professional, 1989.

[27] R. S. Judson, "Genetic algorithms," in *Encyclopedia of Optimization*, C. A. Floudas and P. M. Pardalos, Eds. Springer, Boston, MA, 2009, pp. 1254–1257.

[28] G. Siouris, *Aerospace Avionics Systems: A Modern Synthesis*. Academic Press, 1993.

[29] R. Blanchard, "A new algorithm for computing inertial altitude and vertical velocity," *IEEE T. Aero. Elec. Sys.*, vol. AES-7, no. 6, pp. 1143–1146, 1971.

[30] W. S. Widnall and P. K. Sinha, "Optimizing the gains of the baro-inertial vertical channel," *J. Guid. Control*, vol. 3, no. 2, pp. 172–178, 1980.

[31] D. Titterton and J. Weston, *Strapdown Inertial Navigation Technology*, 2nd ed. The Institution of Engineering and Technology, 2005.

[32] E. Bekir, *Introduction to Modern Navigation Systems*. World Scientific Publishing Company, 2007.

[33] R. M. Rogers, *Applied Mathematics in Integrated Navigation Systems*, 3rd ed. AIAA, 2007.

[34] "IEEE standard for specifying and testing single-axis interferometric fiber optic gyros," *IEEE Std 952-2020 (Revision of IEEE Std 952-1997)*, pp. 1–93, 2021.

[35] D. Allan, "Statistics of atomic frequency standards," *Proc. of the IEEE*, vol. 54, no. 2, pp. 221–230, 1966.

[36] Á. H. A. Maia, F. O. Silva, D. A. de Lima, and R. P. Menezes Filho, "Identificação e modelagem de erros estocásticos em sensores inerciais via variância de Allan e otimização," in *SBAI 2023*, 2022, pp. 1–8.

[37] R. G. Brown and P. Y. C. Hwang, *Introduction to Random Signals and Applied Kalman Filtering with Matlab Exercises*, 4th ed. Wiley, 2012.

[38] J. Hidalgo-Carrió, S. Arnold, and P. Poulakis, "On the design of attitude-heading reference systems using the Allan variance," *IEEE T. Ultrasonics, Ferroelectrics, and Frequency Control*, vol. 63, no. 4, pp. 656–665, 2016.

[39] K. Deb, "Multi-objective evolutionary algorithms," in *Springer Handbook of Computational Intelligence*, J. Kacprzyk and W. Pedrycz, Eds. Springer, Berlin, Heidelberg, 2015, pp. 995–1015.

[40] K. Deb, A. Pratap, S. Agarwal, and T. Meyarivan, "A fast and elitist multiobjective genetic algorithm: NSGA-II," *IEEE T. Evolut. Comput.*, vol. 6, no. 2, pp. 182–197, 2002.

[41] D. de la Fuente, M. A. Vega-Rodríguez, and C. J. Pérez, "Automatic selection of a single solution from the Pareto front to identify key players in social networks," *Knowl.-Based Syst.*, vol. 160, pp. 228–236, 2018.